Journal of Hematology & Oncology

RESEARCH

Open Access

NPM1 inhibits tumoral antigen presentation to promote immune evasion and tumor progression

Xin Wang[1], Yangyang Chai[1], Yuan Quan[1], Jiaming Wang[1], Jiaying Song[1], Wenkai Zhou[1], Xiaoqing Xu[1], Henan Xu[2], Bingjing Wang[1] and Xuetao Cao[1,2*]

Abstract

Background Tumor cells develop multiple mechanisms to facilitate their immune evasion. Identifying tumor-intrinsic factors that support immune evasion may provide new strategies for cancer immunotherapy. We aimed to explore the function and the mechanism of the tumor-intrinsic factor NPM1, a multifunctional nucleolar phosphoprotein, in cancer immune evasion and progression.

Methods The roles of NPM1 in tumor progression and tumor microenvironment (TME) reprogramming were examined by subcutaneous inoculation of *Npm1*-deficient tumor cells into syngeneic mice, and then explored by CyTOF, flow cytometry, immunohistochemistry staining, and RNA-seq. The in-vitro T-cell killing of OVA-presenting tumor cells by OT-1 transgenic T cells was observed. The interaction of NPM1 and IRF1 was verified by Co-IP. The regulation of NPM1 in IRF1 DNA binding to *Nlrc5*, *Ciita* promoter was determined by dual-luciferase reporter assay and ChIP-qPCR.

Results High levels of *NPM1* expression predict low survival rates in various human tumors. Loss of NPM1 inhibited tumor progression and enhanced the survival of tumor-bearing mice. *Npm1*-deficient tumors showed increased $CD8^+$ T cell infiltration and activation alongside the reduced presence of immunosuppressive cells. *Npm1* deficiency increased MHC-I and MHC-II molecules and specific T-cell killing. Mechanistically, NPM1 associates with the transcription factor IRF1 and then sequesters IRF1 from binding to the *Nlrc5* and *Ciita* promoters to suppress IRF1-mediated expression of MHC-I and MHC-II molecules in tumor cells.

Conclusions Tumor-intrinsic NPM1 promotes tumor immune evasion via suppressing IRF1-mediated antigen presentation to impair tumor immunogenicity and reprogram the immunosuppressive TME. Our study identifies NPM1 as a potential target for improving cancer immunotherapy.

Keywords Nucleophosmin, MHC, IRF1, Immune evasion, Tumor microenvironment, Immunosuppression

*Correspondence:
Xuetao Cao
caoxt@immunol.org
[1]Department of Immunology, Center for Immunotherapy, Institute of Basic Medicine, Peking Union Medical College, Chinese Academy of Medical Sciences, Beijing 100005, China
[2]Frontier Research Center for Cell Response, Institute of Immunology, College of Life Sciences, Nankai University, Tianjin 300071, China

Background

Malignant cells have evolved various strategies that promote tumor progression by evading immune recognition and inhibiting the anti-tumor responses, a well-accepted hallmark of cancer [1]. Many tumor-intrinsic changes contribute to immune evasion and lead to resistance to immunotherapies such as immune checkpoint blockade (ICB). These changes include reduced tumor immunogenicity, loss of antigen-presenting molecules, defects in interferon signaling, and implementation of immune-evasive oncogenic signaling pathways [2, 3]. Meanwhile, external factors, such as a reprogrammed immunosuppressive tumor microenvironment (TME), also play important roles in escaping the surveillance of the host immune system and promoting tumor progression. Firing up the immunosuppressive TME might improve the tumor immunogenicity, T cell infiltration or responses and cancer immunotherapy efficacy [4–6]. Therefore, deciphering the hidden mechanisms that support tumor immune evasion and reprogram immunosuppressive TME has the potential to greatly advance our understanding of tumor-host interaction and improve the efficacy of immunotherapy.

The nucleolus is a common nuclear substructure that primarily functions in ribosome biogenesis. Ribosome biogenesis is usually hyperactivated in tumor cells, a significant characteristic of tumors that was identified over a century ago [7]. Nucleolar abnormalities are related to multiple pathologies including cancer [8]. Now, hundreds of nucleolar proteins have been identified through mass-spectrometry analyses of the nucleolar proteome and the functions of these nucleolar proteins are consistent with biological processes that occur within the nucleolus [9, 10]. The nucleolus is membraneless and dynamic, as reflected in the active shuttling of nucleolar proteins between this structure and the surrounding nucleoplasm. Thus, nucleolar proteins have the potential to influence various nuclear functions directly [11]. Up to now, the abnormal expression and mutations of various nucleolar proteins in tumors have been observed. However, whether and how nucleolar proteins function in tumor immune escape remains poorly understood.

Nucleophosmin (NPM1, also known as B23) is one of the most abundant nucleolar proteins and the mutations in the *NPM1* gene are associated with a variety of hematological malignancies, including acute myeloid leukemia (AML) [12]. Some reports have indicated that NPM1 plays an oncogenic role in multiple solid tumors by promoting cell proliferation and inhibiting cell apoptosis [13, 14]. In general, high levels of NPM1 expression have been detected in many solid tumors including colorectal, gastric, hepatocellular and prostate malignancies [12]. However, the contrasting reports suggest that NPM1 inhibits tumor growth by interacting with the tumor suppressor ARF for genomic stability and cell-cycle arrest [15]. To date, only one report has revealed the involvement of NPM1 in tumor immunity and found that NPM1 upregulated PD-L1 transcription in triple-negative breast cancer (TNBC) cells to inhibit T cell activity [16]. Therefore, the potential contribution of NPM1 to tumor progression and immune evasion is worthy of further investigation.

In this study, we find that NPM1 promotes tumor immune evasion by inhibiting tumor antigen presentation and inducing an immunosuppressive TME. Our study reveals the role of tumor-intrinsic NPM1 in immune evasion by targeting NLRC5-MHC-I and CIITA-MHC-II pathways, adding insight into tumor-host interactions and tumor immunogenicity. Our study also identifies NPM1 as a potential target for improving cancer immunotherapy.

Results

Npm1 deficiency suppresses tumor growth in vivo

To examine whether there is a link between NPM1 expression and tumor progression, we first analyzed publicly available data in the TCGA database [17]. Compared to non-tumor samples, *NPM1* mRNA was increased in many human tumor types, including COAD (colon adenocarcinoma), LIHC (liver hepatocellular carcinoma), HNSC (head and neck squamous cell carcinoma), LUAD (lung adenocarcinoma) and KIRP (kidney renal papillary cell carcinoma) (Fig. 1A). In addition, overall survival analysis demonstrated that high levels of *NPM1* predict low survival rates in various human tumors (Fig. 1B). These results indicate that NPM1 promotes human tumor progression.

To characterize the effect of NPM1 on tumor progression and anti-tumor immune responses, we knockout the *Npm1* gene in three mouse tumor cell lines (colon carcinoma MC38, melanoma B16F10 and lung carcinoma LLC) using the CRISPR-Cas9 system (Fig. S1A). The knockout efficacy was confirmed by immunoblotting (Fig. S1B). Wild-type or *Npm1*-deficient tumor cells were then subcutaneously injected into syngeneic wild-type mice, and tumor growth was monitored. We found that loss of NPM1 in MC38 (Fig. 1C and D), B16F10 (Fig. 1E and F) and LLC (Fig. 1G and H) tumor cells significantly reduced tumor growth and prolonged the survival of tumor-bearing mice compared to controls (Fig. 1I and J). Thus, *Npm1* deficiency significantly suppresses tumor growth in multiple mouse tumor models, providing additional evidence that NPM1 promotes tumor progression in vivo.

Npm1 deficiency reprograms the immunogenic tumor microenvironment

To explore the potential function of NPM1 in anti-tumor immune responses, we deciphered the immune

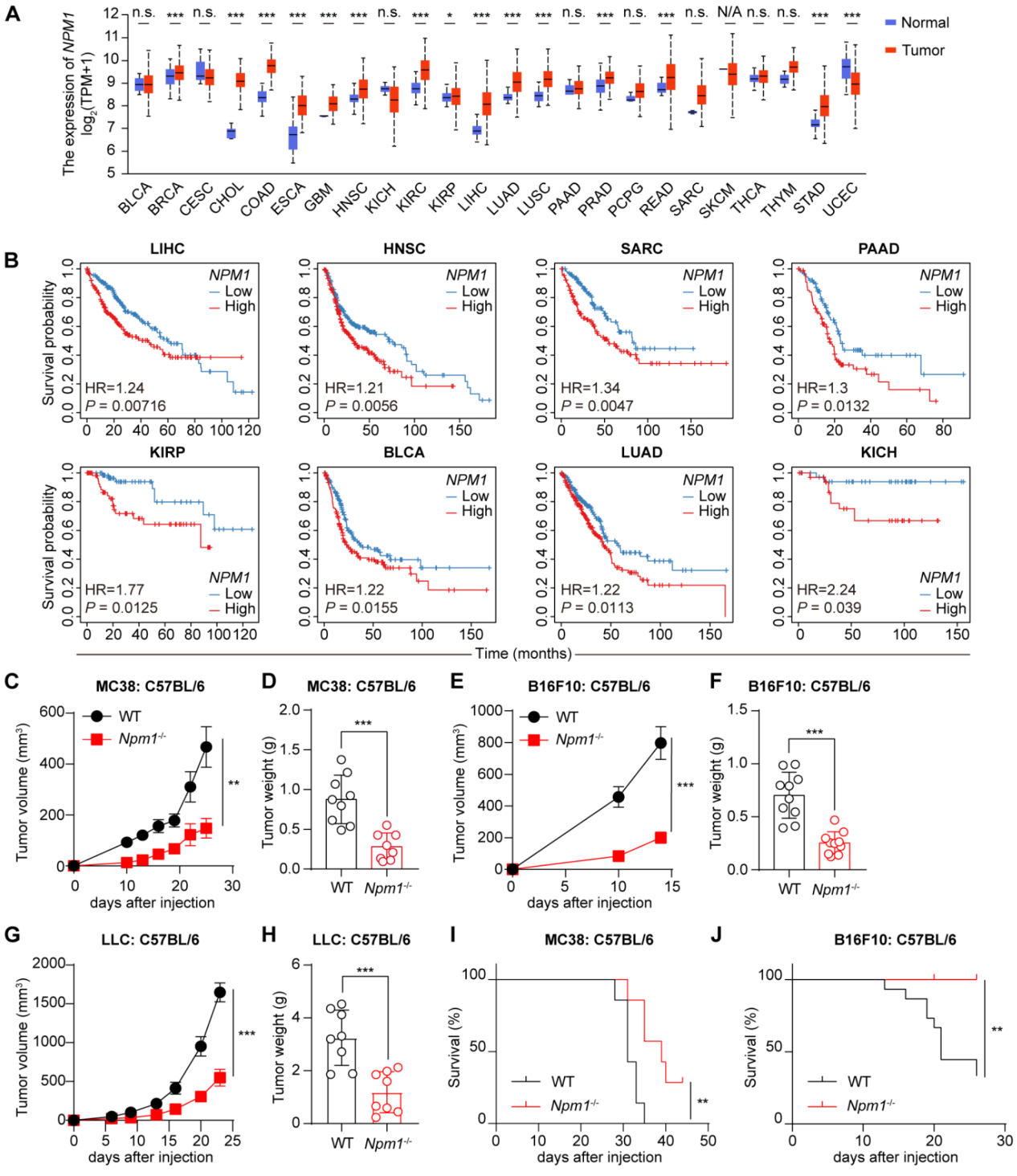

Fig. 1 (See legend on next page.)

atlas of inoculated wild-type and *Npm1*-deficient MC38 tumors using 36-parameter mass cytometry by time of flight (CyTOF) (Fig. 2A). 22 distinct immune cell subsets were identified and the proportion of each immune cell type was calculated using the dimensionality reduction algorithm t-SNE and the clustering algorithm PhenoGraph (Fig. 2B). We found a significant increase in $CD8^+$ T cells (cluster 4) and $CD4^+$ T cells (cluster 7) in *Npm1*-deficient tumors; meanwhile, the macrophage (cluster

(See figure on previous page.)

Fig. 1 NPM1 is linked to increased human and mouse tumor progression. (**A**) Box plots showing the mRNA levels of *NPM1* in different human tumors and the corresponding normal tissues using the TCGA database. (**B**) Kaplan-Meier survival curve for diverse human tumors based on *NPM1* mRNA level using the TCGA database. (**C** and **D**) Wild-type and *Npm1*-deficient MC38 mouse colon cancer cells were subcutaneously injected into syngeneic mice C57BL/6. Tumor growth curve (**C**) and weight at the endpoint (**D**). $n = 6$, 5 mice, respectively in **C**. $n = 9$, 8 mice, respectively in **D**. (**E** and **F**) Wild-type and *Npm1*-deficient B16F10 mouse melanoma cells were subcutaneously injected into C57BL/6 mice. Tumor growth curve (**E**) and weight at the endpoint (**F**). $n = 9$, 10 mice, respectively in **E**. $n = 10$ mice per group in **F**. (**G** and **H**) Wild-type and *Npm1*-deficient LLC mouse lung carcinoma cells were subcutaneously injected into C57BL/6 mice. Tumor growth curve (**G**) and weight at the endpoint (**H**). $n = 7$ mice per group in **G**. $n = 8$ mice per group in **H**. **(I)** Overall survival of MC38 tumor-bearing mice. $n = 7$ mice per group. (**J**) Overall survival of B16F10 tumor-bearing mice. $n = 15$, 11 mice, respectively. Data are representative of three independent experiments (**C**-**H**); data are combined results from two separate experiments (**I** and **J**). Error bars in **A**, **D**, **F** and **H** indicate mean ± SD; error bars in **C**, **E** and **G** indicate mean ± SEM. *P* values in **A**, **D**, **F** and **H** were calculated by a two-tailed, unpaired Student's *t* test; *P* values in **C**, **E** and **G** were calculated by two-way ANOVA; *P* values in **B**, **I** and **J** were analyzed by log-rank test. $^{*}P < 0.05$; $^{**}P < 0.01$; $^{***}P < 0.001$. n.s., not significant; N/A, not applicable; HR, hazard ratio. BLCA, bladder urothelial carcinoma; BRCA, breast invasive carcinoma; CESC, cervical squamous cell carcinoma and endocervical adenocarcinoma; CHOL, cholangiocarcinoma; COAD, colon adenocarcinoma; ESCA, esophageal carcinoma; GBM, glioblastoma multiforme; HNSC, head and neck squamous cell carcinoma; KICH, kidney chromophobe; KIRC, kidney renal clear cell carcinoma; KIRP, kidney renal papillary cell carcinoma; LIHC, liver hepatocellular carcinoma; LUAD, lung adenocarcinoma; LUSC, lung squamous cell carcinoma; PAAD, pancreatic adenocarcinoma; PRAD, prostate adenocarcinoma; PCPG, pheochromocytoma and paraganglioma; READ, rectum adenocarcinoma; SARC, sarcoma; SKCM, skin cutaneous melanoma; THCA, thyroid carcinoma; THYM, thymoma; STAD, stomach adenocarcinoma; UCEC, uterine corpus endometrial carcinoma. See also Figure S1

1 and 19) and myeloid-derived suppressor cell (MDSC) (cluster 17) populations were reduced (Fig. 2C).

Since the recruitment and activation of cytotoxic T cells in the TME is essential for eliciting an effective anti-tumor response [4], we next investigated the expression profiles of each T cell cluster using CyTOF analysis (Fig. 2D). Specifically, $CD8^+$ T cells in cluster 2, a group that was increased in the *Npm1*-deficient TME, expressed the highest levels of the cytotoxic effector molecules perforin, granzyme B and IFN-γ, as well as the co-stimulatory molecules CD28 and CD86. This profile indicates the enhanced infiltration of effector $CD8^+$ T cells in the *Npm1*-deficient TME. $CD8^+$ T cells in cluster 4 showed high expression of Ly6C, CD28 and CD86 and were also significantly increased in the *Npm1*-deficient TME. Notably, $Ly6C^+$ $CD8^+$ T cells have been reported to exhibit a more activated state and correlate with enhanced cytotoxic activity [18]. $CD4^+$ T cells in cluster 6 were defined as the regulatory T cells (Tregs) since they co-express FoxP3 and CD25. There was no significant difference in this cluster between the wild-type and *Npm1*-deficient TME. $CD4^+$ T cells in cluster 7 were significantly increased in the *Npm1*-deficient TME. However, we could not define the specific subtype represented by cluster 7 due to antibody panel limitations.

In addition to T cells, we defined cluster 1 and cluster 19 as the inhibitory macrophages since they express high levels of F4/80 and Arginase 1. Meanwhile, cluster 10 and cluster 17 were characterized by high expression of Ly6C and thus defined as MDSCs. All of these myeloid cells, which play roles in immunosuppression in the TME, were significantly decreased in *Npm1*-deficient tumors (Fig. 2C). Furthermore, *Npm1* deficiency resulted in reduced expression of genes associated with immune suppression in myeloid cells, such as CD11b, F4/80, Arginase 1 and Ly6C (Fig. 2E).

In summary, CyTOF analysis of MC38 tumors indicates that *Npm1* deficiency inflames the TME to be immunogenic by promoting the infiltration, activation of $CD8^+$ T cells, $CD4^+$ T cells and inhibiting immunosuppressive phenotypes, thereby boosting anti-tumor immune responses.

Npm1 deficiency promotes $CD8^+$ T cell infiltration into tumors

Flow cytometry analysis confirmed that $CD45^+$ immune cell infiltration and the proportion of $CD4^+$ T cells and $CD8^+$ T cells were increased in *Npm1*-deficient MC38 tumors (Fig. 3A) and LLC tumors (Fig. 3B) compared to controls. Meanwhile, the proportion of natural killer cells (NKs) and DCs showed no significant differences in MC38 tumors (Fig. S2A, S2B) and LLC tumors (Fig. S3A, S3B); only the proportion of MDSCs was decreased in *Npm1*-deficient LLC tumors (Fig. S3A) in flow cytometry analysis. Immunohistochemistry (IHC) staining confirmed a consistent and significant increase in $CD8^+$ T cell infiltration into *Npm1*-deficient MC38 tumors (Fig. 3C).

To determine the contribution of enhanced infiltration of $CD8^+$ T cells to tumor inhibition in *Npm1*-deficient tumors, we utilized an antibody-based $CD8^+$ T cell depleting approach and found that $CD8^+$ T cell depletion strikingly abolished the growth delay of *Npm1*-deficient tumors (Fig. 3D).

Furthermore, to account for deviations caused by tumor size, we subcutaneously injected wild-type and *Npm1*-deficient tumor cells on the same day but resected them five days apart to equalize the tumor size at the experimental endpoint (Fig. 3E). Subsequent CyTOF analysis recapitulated the differences in immune cell infiltration into the TME, including a significant enrichment of $CD8^+$ T cells, $CD4^+$ T cells and DCs but decreased numbers of several tumor-associated macrophage (TAM) subsets in *Npm1*-deficient tumors compared to controls (Fig. 3F and G).

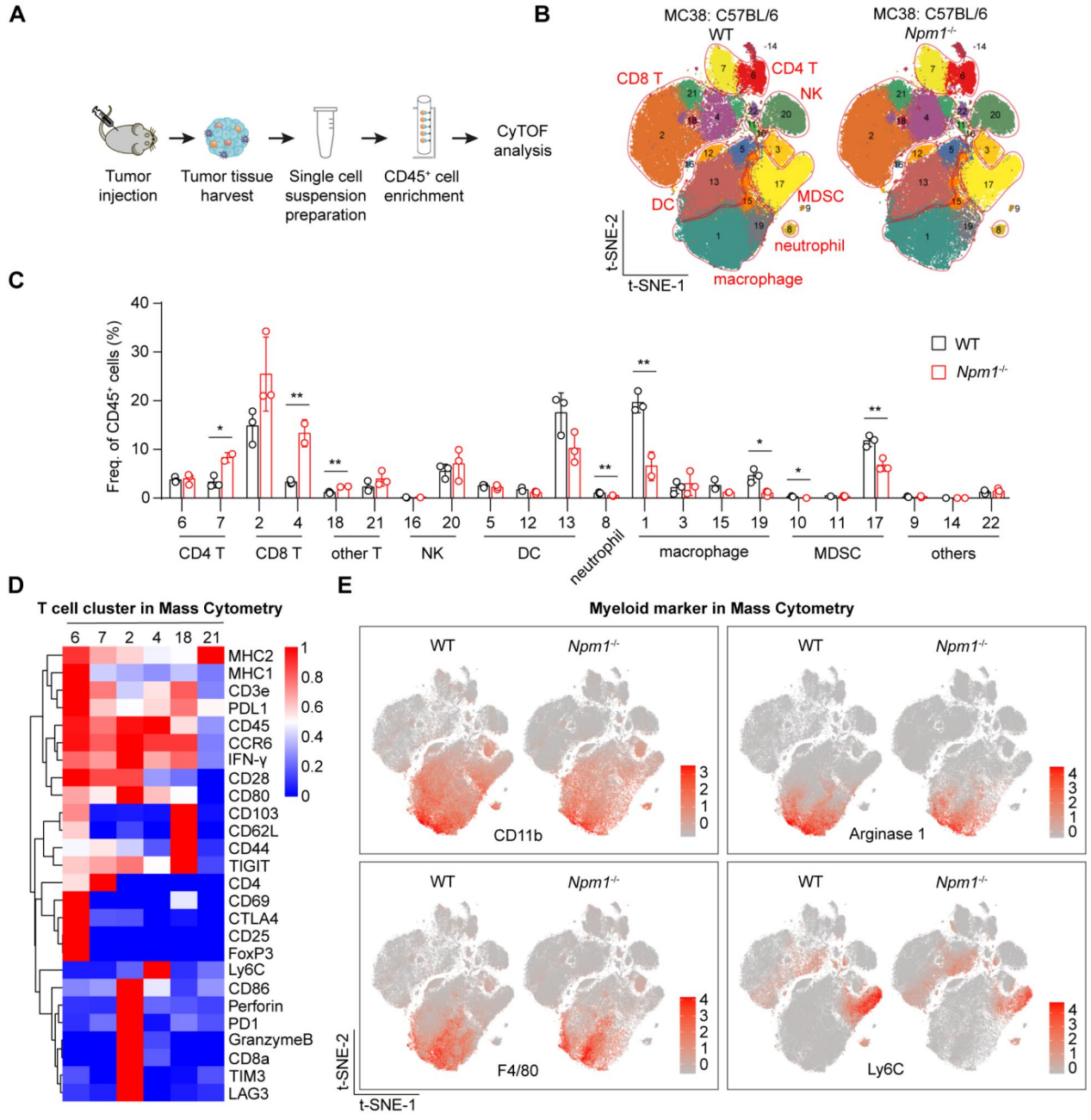

Fig. 2 *Npm1* deficiency in tumor cells leads to an inflammatory and immunogenic profile in the TME. (**A**) Schematic diagram of CyTOF experiments. MC38 tumor cells were subcutaneously injected into C57BL/6 mice. Tumor tissues were collected on day 25 and digested into a single-cell suspension. $CD45^+$ cells were isolated using magnetic beads and labeled for CyTOF analysis. $n = 8$ mice per group. (**B**) t-SNE plot of 180,000 $CD45^+$ singlets collected and analyzed as in (**A**). (**C**) The frequencies of each PhenoGraph cluster to $CD45^+$ immune cells as in (**A**). (**D**) Heatmap showing the normalized expression profiles of the T cell PhenoGraph clusters as in (**A**). (**E**) Normalized expression of indicated myeloid markers on the t-SNE plot as in (**A**). Data are representative of two independent experiments. Error bars in **C** indicate mean ± SD. *P* values in **C** were calculated by a two-tailed, unpaired Student's *t* test. $^*P < 0.05$; $^{**}P < 0.01$

These results further demonstrate that *Npm1* deficiency reprograms the immunogenic TME by promoting the infiltration of $CD8^+$ T cells, which then control the growth of *Npm1*-deficient tumors.

Npm1 deficiency enhances tumor cell MHC expression and immunogenicity

Next, we wondered how *Npm1* deficiency reprograms the immunogenic TME. We determined the effect of tumor NPM1 on in-vitro CTL-dependent killing of

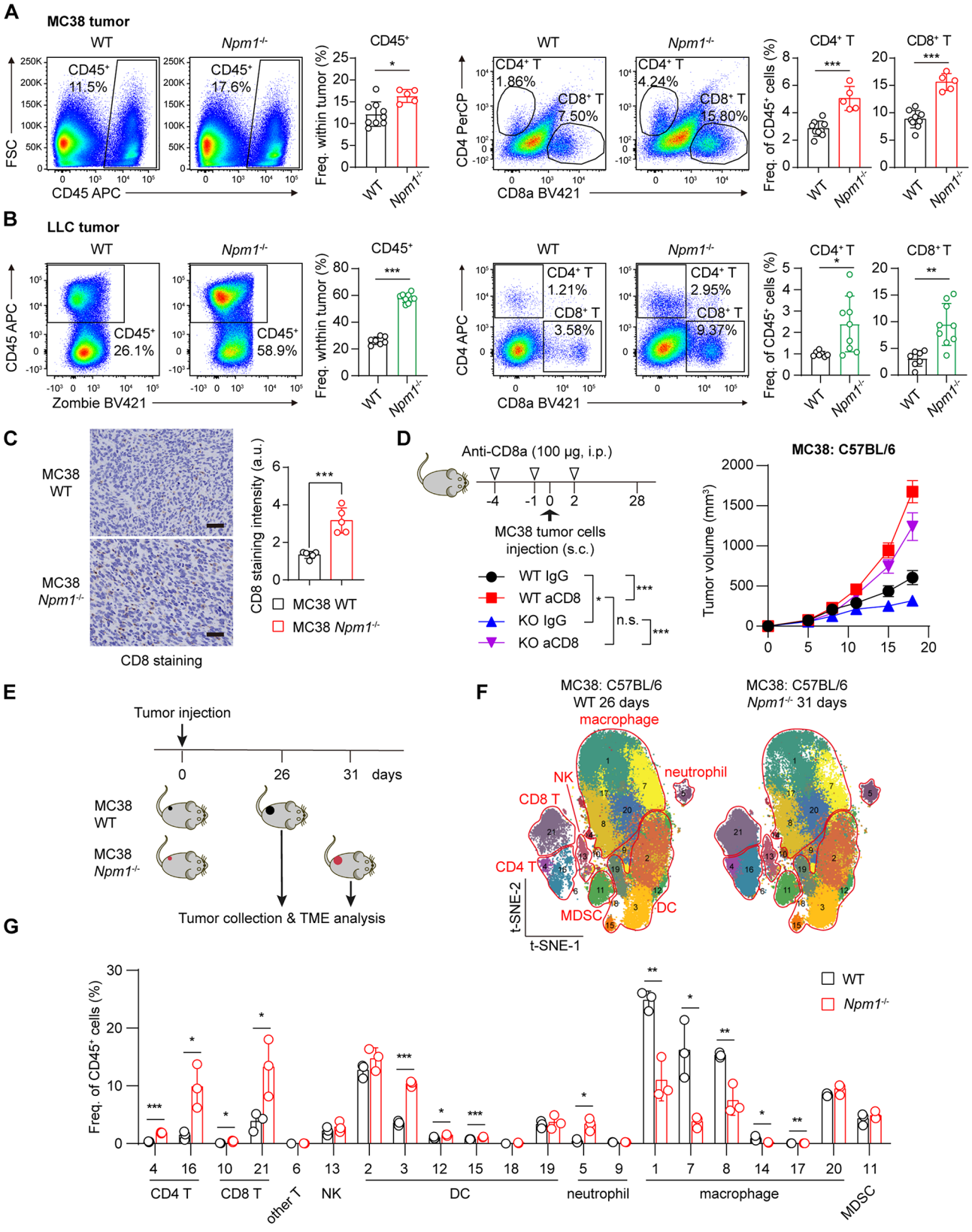

Fig. 3 (See legend on next page.)

(See figure on previous page.)

Fig. 3 *Npm1* deficiency in tumor cells enhances the infiltration of $CD8^+$ T cells in the TME. (**A**) Flow cytometry analysis of the percentage of $CD45^+$ immune cells, $CD4^+$ T cells and $CD8^+$ T cells in MC38 tumors. Representative FACS plots (left) with quantification (right) were shown. $n = 9$, 5 mice, respectively. (**B**) Flow cytometry analysis of the percentage of $CD45^+$ immune cells, $CD4^+$ T cells and $CD8^+$ T cells in LLC tumors. Representative FACS plots (left) with quantification (right) were shown. $n = 7$, 9 mice, respectively. (**C**) Immunohistochemistry (left) with quantification (right) of $CD8^+$ T cells in MC38 tumors. $n = 5$ mice per group. Scale bar, 10 μm. (**D**) Schematic diagram of lymphocyte depletion experiment (left) and tumor growth curve of tumor-bearing mice (right). MC38 tumor cells were subcutaneously injected into C57BL/6 mice on day 0 when $CD8^+$ T cells were depleted using 100 μg of intraperitoneally injected anti-CD8 antibody on days −4, -1 and 2. $n = 8$ mice per group. (**E**) Schematic diagram showing the mouse tumor model in which wild-type or *Npm1*-deficient MC38 tumor cells were subcutaneously injected into C57BL/6 mice and resected five days apart to equalize tumor size. $n = 8$ mice per group. (**F**) t-SNE plot of 180,000 $CD45^+$ singlets collected and analyzed as in (**E**). (**G**) The frequencies of each PhenoGraph cluster to $CD45^+$ immune cells as in (**E**). Data are representative of three independent experiments (**A** and **B**). Error bars indicate mean ± SD. *P* values in **A**, **B**, **C** and **G** were calculated using a two-tailed, unpaired Student's *t* test; *P* values in **D** were calculated by two-way ANOVA. $^*P < 0.05$; $^{**}P < 0.01$; $^{***}P < 0.001$. a.u., arbitrary unit; i.p., intraperitoneal; s. c., subcutaneous. See also Figure S2 and Figure S3

OVA-presenting tumor cells by OT-I transgenic T cells which specifically recognize SIINFEKL OVA peptides. We found that *Npm1*-deficient tumor cells were significantly more sensitive than wild-type tumors to specific T-cell killing (Fig. 4A and B).

We went further to conduct a transcriptomic analysis to comprehensively compare gene expression in wild-type and *Npm1*-deficient tumor cells freshly isolated from MC38 tumor tissues. Gene ontology (GO) analysis of the up-regulated genes in the *Npm1*-deficient tumor cells showed that three of the top ten biological processes were associated with antigen processing and presentation (Fig. 4C). Gene-set enrichment analysis (GSEA) showed that two gene sets, the antigen processing and presentation of exogenous antigen (GO: 0019884) and the antigen processing and presentation of peptide or polysaccharide antigen via MHC class II pathway (GO: 0002504), were significantly enriched in *Npm1*-deficient tumor cells (Fig. 4D).

The RNA-seq results were confirmed by Q-PCR analysis of MHC-I (*H2-D1*, *H2-K1* and *Tap1*) and MHC-II (*Cd74*, *H2-Eb1* and *H2-Dmb1*) transcripts. These mRNAs were significantly elevated in *Npm1*-deficient tumor cells freshly isolated from inoculated tumors (Fig. 4E). Flow cytometry analysis validated that both MHC-I and MHC-II expression were significantly increased in *Npm1*-deficient tumors relative to control tumors (Fig. 4F). To further verify the relationship between NPM1 and MHC expression, we pretreated MC38 tumor cells with mIFN-γ in vitro and found that *Npm1* deficiency resulted in a marked increase in MHC-I and MHC-II expression at the mRNA and protein levels (Fig. 4G and H). Consistent results were obtained by analyses of B16F10 tumor cells (Fig. S4A, S4B) and LLC tumor cells (Fig. S4C, S4D), both were treated with mIFN-γ in vitro. Consistently, siRNA-mediated silencing of *NPM1* significantly enhanced hIFN-γ-induced MHC-I and MHC-II expression in human lung cancer cells A549 (Fig. 4I and J) and human colon cancer cells HCT116 (Fig. S4E-S4G). Furthermore, analysis of TCGA data [19] revealed that MHC class I molecules (*HLA-A*, *HLA-B*, *HLA-C* and *TAPBP*) (Fig. S5A) and MHC class II molecules (*HLA-DPB1*, *HLA-DQA1*, *HLA-DQA2* and *HLA-DRB1*) (Fig. S5B) were negatively associated with *NPM1* mRNA levels in human COAD and SKCM (skin cutaneous melanoma).

Taken together, these results demonstrate that *Npm1* deficiency leads to increased MHC-I and MHC-II expression, which may underline the increased antigen processing and presentation of tumor cells, and also promote tumor immunogenicity and support cytotoxic T cell-mediated elimination of tumor cells.

Npm1 deficiency increases the transcription of *Nlrc5* and *Ciita* in tumor cells

NLRC5 and CIITA have been recognized as master transcription factors regulating the MHC-I and MHC-II genes, respectively [20, 21]. Consistent with this, we found a negative correlation between *NPM1* mRNA levels and *NLRC5* and *CIITA* in multiple human tumors including SKCM, TGCT (testicular germ cell tumors), GBM (glioblastoma multiforme) and LGG (brain lower grade glioma) in TCGA data (Fig. 5A). Consistently, we observed the in vivo expression of *Nlrc5* and *Ciita* were significantly enhanced in *Npm1*-deficient tumors (Fig. 5B and C). Meanwhile, the mRNA levels of *Nlrc5* and *Ciita* were also significantly increased in mIFN-γ-treated *Npm1*-deficient MC38 cells (Fig. 5D) and in hIFN-γ-treated *NPM1*-silenced A549 cells (Fig. 5E) in vitro. These results indicate that *Npm1* deficiency upregulates MHC expression, possibly by affecting the abovementioned upstream transcription factors.

Since *Npm1* deficiency resulted in increased mRNA levels of *Nlrc5* and *Ciita*, we tested whether NPM1 acts at the transcriptional or post-transcriptional level. We treated tumor cells with IFN-γ and found that *Npm1* deficiency significantly increased the preRNA levels of *Nlrc5* and *Ciita*(Fig. 5F). However, by measuring the half-life of the *Nlrc5* and *Ciita* mRNAs in tumor cells treated with actinomycin D, we found that the stability of these transcripts was unaffected by the presence or absence of NPM1 (Fig. 5G). Therefore, NPM1 regulates *Nlrc5* and *Ciita* expression at the transcriptional level.

In addition, we explored the effect of the NPM1 inhibitor NSC348884, which disrupted the oligomerization

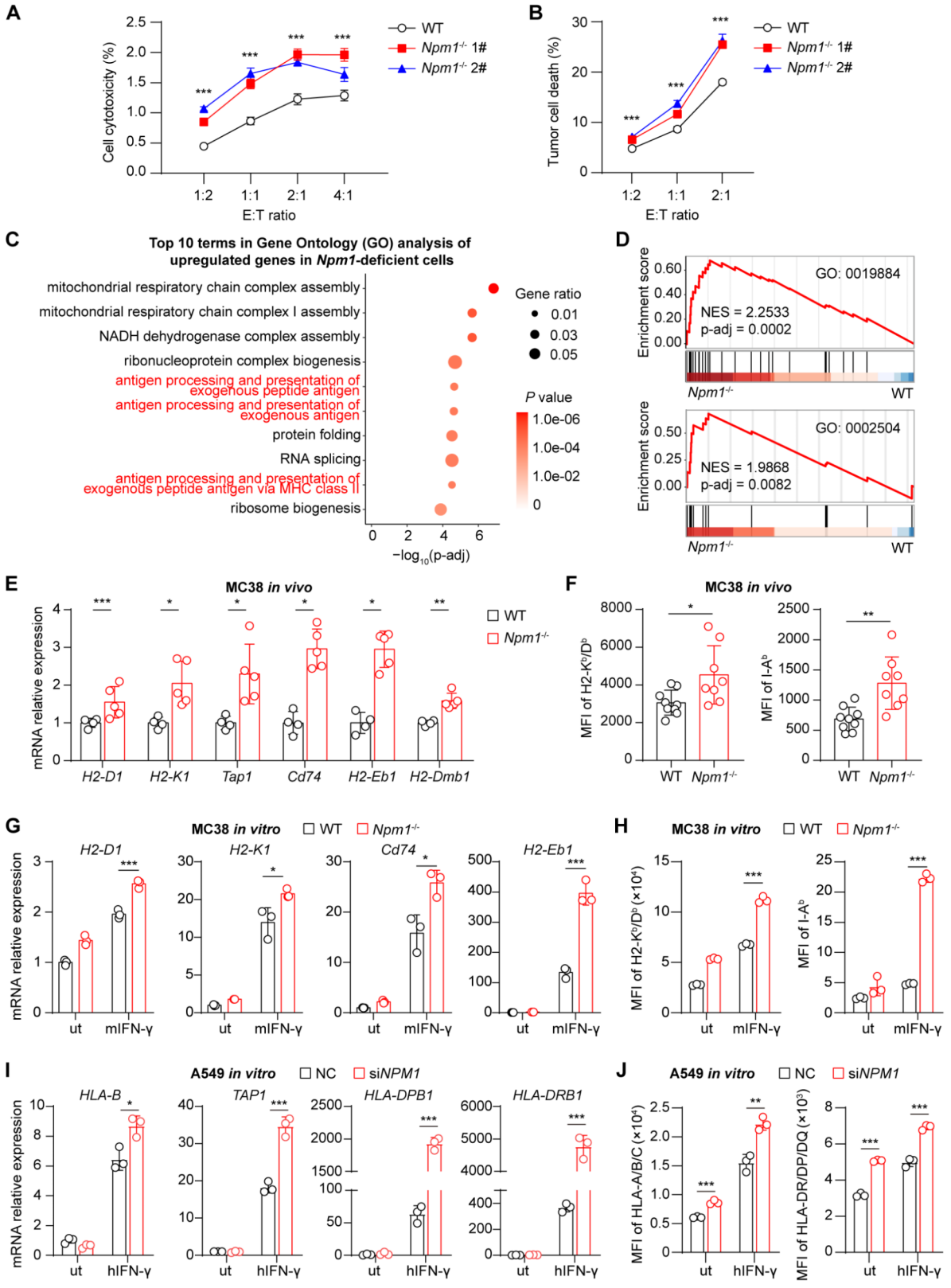

Fig. 4 (See legend on next page.)

(See figure on previous page.)

Fig. 4 *Npm1* deficiency enhances specific T-cell killing and MHC expression in tumor cells. (**A**) LDH cytotoxicity assay of MC38 tumor cells incubated with activated OVA-specific T cells at decreasing E: T ratios (1:2, 1:1, 2:1 and 4:1) for 24 h. $n = 3$. (**B**) Flow cytometry analysis of the fraction of PI^+ MC38 tumor cells incubated with activated OVA-specific T cells at decreasing E: T ratios (1:2, 1:1 and 2:1) for 24 h. $n = 3$. (**C** and **D**) Transcriptomic analysis of $CD45^-$ tumor cells isolated from wild-type and *Npm1*-deficient MC38 tumors. The top 10 enriched biological processes in GO analysis (**C**) and GSEA plots of antigen processing and presentation gene signatures (**D**) are shown. (**E** and **F**) Q-PCR analysis of the mRNA levels of MHC genes (**E**) and flow cytometry analysis of H2-K^b/D^b and I-A^b levels (**F**) of wild-type and *Npm1*-deficient MC38 tumor cells isolated from subcutaneous tumors. $n = 4$, 5 mice, respectively in **E**. $n = 9$, 8 mice, respectively in **F**. (**G** and **H**) Q-PCR analysis of the mRNA levels of MHC genes (**G**) and flow cytometry analysis of H2-K^b/D^b and I-A^b levels (**H**) of wild-type and *Npm1*-deficient MC38 tumor cells treated with mIFN-γ (10 ng/mL) for 48 h in vitro. $n = 3$. (**I** and **J**) Q-PCR analysis of the mRNA levels of MHC genes (**I**) and flow cytometry analysis of HLA-A/B/C and HLA-DR/DP/DQ levels (**J**) in A549 cells transfected with siNC or si*NPM1* for 48 h and then treated with hIFN-γ (20 ng/mL) for 24 h. $n = 3$. Data shown are representative of three independent experiments (**A**, **B** and **E**-**J**). Error bars indicate mean ± SD. *P* values were calculated using a two-tailed, unpaired Student's *t* test. $^*P < 0.05$; $^{**}P < 0.01$; $^{***}P < 0.001$. E: T ratio, effector: target ratio; NES, normalized enrichment score; MFI, mean fluorescence intensity; ut, untreated; NC, negative control. See also Figure S4 and S5

of NPM1 but did not change NPM1 protein levels, on MHC expression of tumor cells [22]. Our data revealed that NSC348884 did not affect the MHC expression in MC38, B16F10, A549 and HCT116 tumor cells (Fig. S6). We therefore hypothesized that NPM1 oligomerization is not related to its regulation of MHC expression in tumor cells.

NPM1 associates with IRF1 and inhibits IRF1-mediated *Nlrc5* and *Ciita* transcription

It is well established that IRF1 and STAT1 are key factors required for the transcriptional induction of MHC antigen-presenting genes upon IFN-γ stimulation [2, 3]. Previous researches show that NPM1 interacts with IRF1 and STAT1 [23] and NPM1 inhibits the DNA-binding and transcriptional activity of IRF1 [24]. Indeed, immunoprecipitation assays confirmed that NPM1 could associate with IRF1 and STAT1 as reported (Fig. 6A). We examined the subcellular location of NPM1 protein and found that NPM1 was mainly localized in the nucleolus (Fig. 6B). Subcellular fractionation analysis revealed that NPM1 was widely distributed in the nucleus, including nucleoplasm and chromatin (Fig. 6C). Notably, NPM1 was abundant in chromatin fraction, implying NPM1 might regulate gene transcription. Therefore, we constructed luciferase reporter plasmids bearing the core promoter region of either the *Nlrc5* or the *Ciita* gene. Using the dual-luciferase reporter assay, we discovered that the activity of both the *Nlrc5* and *Ciita* promoter was increased in *Npm1*-deficient cells compared to controls (Fig. 6D). By performing chromatin immunoprecipitation (ChIP) assays, we noticed that *Npm1* deficiency greatly enhanced the binding of IRF1 to the promoter of *Nlrc5* and *Ciita* in IFN-γ stimulated tumor cells (Fig. 6E). However, we observed no significant effect of NPM1 on STAT1 binding (Fig. 6F). Our data indicate that NPM1 interacts with IRF1 to block its binding to the *Nlrc5* and *Ciita* promoters and thus inhibit their transcription, leading to MHC downregulation and, ultimately, immune evasion (Fig. 6G).

Discussion

Tumor cells have evolved various mechanisms that support immune evasion and immunotherapy resistance. Indeed, loss of MHC antigen presentation is one of the most common tumor immune evasion mechanisms [2, 3]. Genetic mutation on MHC gene locus [25], transcriptional or epigenetic downregulation of MHC expression [26, 27] and post-translational degradation of MHC molecules [28, 29] have been broadly implicated in tumor immune evasion and resistance to ICB therapy. Meanwhile, the reprogrammed, immunosuppressive TME has been recognized as a crucial determinant of ICB therapeutic efficacy [4, 5]. Altered immune cell composition [30–32], innate immune sensing pathways [33, 34], cellular metabolism [35–37] and epigenetic factors [6, 38, 39] are involved in modulating the TME. However, the tumor intrinsic mechanisms that target MHC antigen presentation to reprogram the immunosuppressive TME remain incomplete, and a comprehensive understanding of the regulation of MHC molecules will provide promising targets to facilitate ICB therapy. Here we find that genetic depletion of *Npm1* restores MHC-mediated antigen presentation in tumor cells and effectively induces $CD8^+$ T cell infiltration into the TME, suggesting that NPM1 promotes tumor progression and supports tumor immune evasion. Mechanistically, NPM1 inhibits MHC expression by blocking IRF1 binding to the *Nlrc5* and *Ciita* promoters. *Nlrc5* and *Ciita* are IFN-inducible genes encoding transactivators that selectively bind MHC-I and MHC-II gene promoters, respectively. IRF1 is a key regulator of IFN-mediated gene expression and is required for *Nlrc5* and *Ciita* gene transcription. Our study reveals a previously uncharacterized function of NPM1, an archetypal nucleolar protein, in tumor antigen presentation and immune evasion, contributing to a better understanding of tumor-host interactions.

$CD8^+$ cytotoxic T cells are the strongest effector in anti-tumor immune responses. Multiple cancer immunotherapies are developed based on the molecular and cellular biology of the $CD8^+$ T cells [40]. For example, immune checkpoint blockade therapies are designed to target co-inhibitory receptors that suppress $CD8^+$ T cell

responses; and adoptive cell transfer therapies (ACT) are designed to genetically modify chimeric antigen receptors (CAR) to enhance $CD8^+$ T cell function [41, 42]. The expression of MHC molecules increases the immune recognition of tumors. In general, MHC-I molecules present endogenous antigens to prime $CD8^+$ T cells; whereas $CD4^+$ T cells recognize exogenous antigens presented by MHC-II molecules which are mainly expressed in antigen-presenting cells. Tumor-specific MHC-II (tsMHC-II) expression is associated with favorable clinical outcomes and better response rates to ICB therapy in cancer patients [43, 44]. MHC-II-restricted antigens are important to activate $CD4^+$ T cell responses, which further support the anti-tumor responses of $CD8^+$ T cells [29, 45]. In this study, we reveal that NPM1 inhibits the transcription of both NLRC5-MHC-I and CIITA-MHC-II pathways via suppressing their common upstream transcription factor IRF1, highlighting a novel regulation axis of NPM1-IRF1-NLRC5/CIITA-MHC that modulates tumor antigen presentation and reprograms the TME. Our CyTOF and FACS analysis consistently reveal that loss of NPM1 significantly enhanced the infiltration of both $CD8^+$ T cells and $CD4^+$ T cells into the TME and enhanced the anti-tumor responses of T cells in the TME. We demonstrate the critical role of the enhanced $CD8^+$ T cells in inhibiting *Npm1*-deficient tumors through depletion of $CD8^+$ T cells in vivo and CTL-dependent killing assay in vitro. Recently, the crucial roles of $CD4^+$ T cells in cancer immunotherapy have also been revealed [46, 47]. Distinct subsets of $CD4^+$ T cells have been identified in the TME and antigen-specific $CD4^+$ T cells are shown to be critical for anti-tumor effects, which display a T_H1 phenotype [45]. However, our in-vivo data showed that the depletion of $CD8^+$ T cells almost completely abolished the anti-tumor effects of *Npm1* deficiency, indicating the crucial roles of $CD8^+$ T cells in mediating the eradication of *Npm1*-deficient tumors. Thus, we hypothesized that although $CD4^+$ T cell infiltration is increased in *Npm1*-deficient TME, the $CD4^+$ T cells are more likely to play a helper role by assisting $CD8^+$ T cell activation.

Over the past decades, our understanding of the function of nucleolus in ribosome biogenesis has advanced considerably [7]. Moreover, emerging studies showed that numerous stress stimuli, such as chemotherapeutic agents, hypoxia, oxidation state and an acidic environment, might induce nucleocytoplasmic translocation of certain nucleolar proteins and activate p53-dependent nucleolar stress pathway [48]. Activation of the nucleolar stress pathway can lead to cell-cycle arrest, apoptosis, DNA damage and cell senescence, suggesting that targeting the nucleolar stress pathway may contribute to the treatment of malignant diseases [49]. Recent evidences have also uncovered new roles of the nucleolus in biological processes, including protein quality control [50], RNA editing [51, 52], DNA repair [53] and liquid-liquid phase separation (LLPS) [54]. Changes in nucleolar morphology and activity have been associated with numerous human diseases, providing promising therapeutic potentials for targeting nucleoli [8]. NPM1 is the most abundant protein in the nucleolus and is important for maintaining nucleolar organization and function [14, 55]. NPM1 has active nucleolus-nucleoplasm shuttling activity and participates in various biological processes as a molecular chaperone, such as histone chaperone and DNA- or RNA-binding protein. Previous studies report that NPM1 is a proto-oncogene via stimulating cell proliferation and preventing apoptosis [13, 14]; oppositely, NPM1 has been reported as a tumor suppressor gene because it contributes to genome stability control and growth-suppressing pathways [15]. However, these researches usually focus on NPM1's roles in tumor biology, but not on tumor-host interaction and tumor immunity [56, 57]. Here we have addressed the role of NPM1 in tumor immune evasion and immunosuppressive TME reprogramming and also validated its pro-tumor roles using multiple in-vivo mouse tumor models. We found that a small amount of NPM1 is distributed in the nucleoplasm and chromatin components, where NPM1 sequesters transcription factor IRF1 from binding to the *Nlrc5* and *Ciita* promoters to suppress the expression of MHC molecules, thus impairing tumor immunogenicity. A study also reveals that NPM1 upregulates the transcription of PD-L1 and suppresses tumor immunogenicity in triple-negative breast cancer [16]. A better understanding of the underlying mechanism of NPM1 in regulating tumor immunogenicity might help to enhance immunotherapy responses by targeting nucleolar proteins.

Almost all cancer immunotherapies, such as ICB inhibitors, ACT therapy, recombinant cytokines and innate TLR agonists inhibit cancer progression by modulating IFN-γ signaling. Therefore, the exploration of novel regulators of IFN-γ signaling will open up new avenues for immunotherapies. Our study found that tumoral NPM1 inhibits IFN-γ-induced MHC expression and tumor immunogenicity, which could be the cause of immunotherapy resistance. Our results are consistent with the clinical observation that high expression of NPM1 predicts low survival rates in various human solid tumors [12]. Hence, reducing the expression of NPM1 in tumor cells by small molecule inhibitors, antisense oligonucleotides or proteolysis targeting chimeras (PROTACs) technology may be a promising strategy to unleash the resistance and improve the efficacy of cancer immunotherapy. It has been reported that NPM1 inhibitor NSC348884 disrupts the oligomerization of NPM1 protein without affecting NPM1's protein level [22]. However, we found that NSC348884 did not affect the expression of MHC in several tumor cells in vitro. A

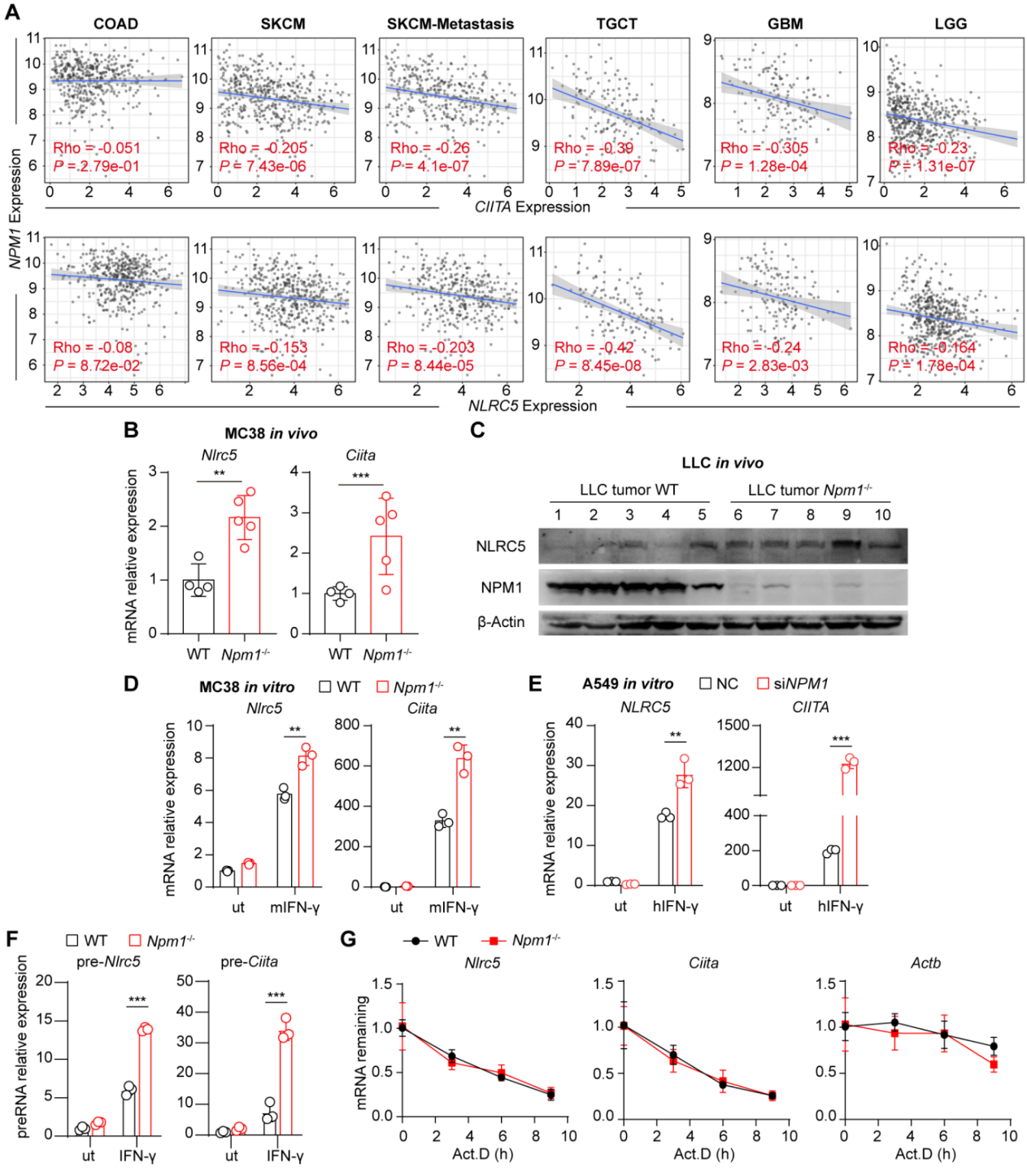

Fig. 5 *Npm1* deficiency promotes the transcription of *Nlrc5* and *Ciita*. (**A**) Correlation of *NPM1* with *CIITA* (upper) or *NLRC5* (bottom) in different cancer types. Data were obtained from TCGA and analyzed by the Spearman correlation test. (**B**) Q-PCR analysis of the mRNA levels of *Nlrc5* and *Ciita* in wild-type and *Npm1*-deficient MC38 tumors cells isolated from subcutaneous tumors. $n = 4$, 5 mice, respectively. (**C**) Immunoblot analysis of NLRC5 expression in wild-type and *Npm1*-deficient LLC tumor tissues. Uncropped blots are shown in the source data. (**D**) Q-PCR analysis of the mRNA levels of *Nlrc5* and *Ciita* in wild-type and *Npm1*-deficient MC38 tumor cells treated with mIFN-γ (10 ng/mL) for 48 h in vitro. $n = 3$. (**E**) Q-PCR analysis of the mRNA levels of *NLRC5* and *CIITA* in A549 cells transfected with siNC or si*NPM1* for 48 h and then treated with hIFN-γ (20 ng/mL) for 24 h. $n = 3$. (**F**) Q-PCR analysis of the preRNA levels of *Nlrc5* and *Ciita* in mIFN-γ-treated (10 ng/mL) wild-type and *Npm1*-deficient MC38 tumor cells in vitro. $n = 3$. (**G**) Decay curves of *Nlrc5*, *Ciita* and *Actb* mRNAs in mIFN-γ-stimulated wild-type and *Npm1*-deficient MC38 tumor cells treated with actinomycin D (10 μg/mL) for 0, 3, 6 and 9 h. $n = 3$. Data are representative of three independent experiments (**B**, **D**-**G**). Error bars indicate mean ± SD. *P* values in **A** were calculated using the Spearman correlation test; *P* values in **B**, **D**-**G** were calculated using a two-tailed, unpaired Student's *t* test. $^{*}P < 0.05$; $^{**}P < 0.01$; $^{***}P < 0.001$. ut, untreated; NC, negative control; Act. D, actinomycin D. See also Figure S6

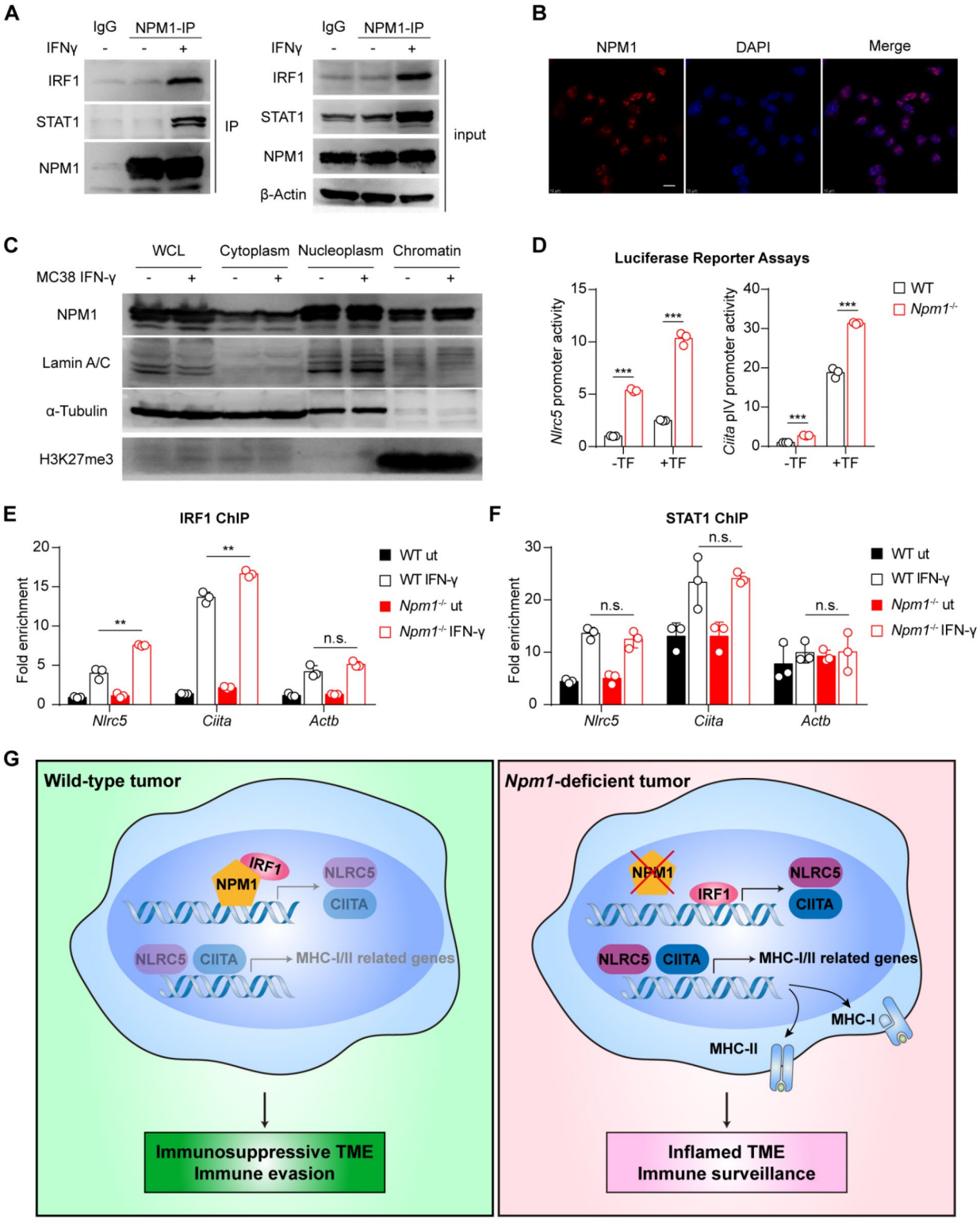

Fig. 6 (See legend on next page.)

(See figure on previous page.)

Fig. 6 NPM1 inhibits MHC expression by interacting with IRF1 and blocking IRF1 binding to *Nlrc5* and *Ciita* promoters. (**A**) Immunoprecipitation analysis of the interaction between NPM1 and IRF1 and STAT1 in MC38 tumor cells treated with mIFN-γ (10 ng/mL) for 24 h. Uncropped blots are shown in the source data. (**B**) Immunofluorescence analysis of the subcellular location of NPM1 in MC38 tumor cells. Scale bar, 10 μm. (**C**) Subcellular fractionation of MC38 tumor cells with or without mIFN-γ treatment (10 ng/mL) for 24 h. Each fraction was loaded in equal proportions. Uncropped blots are shown in the source data. (**D**) Dual-luciferase reporter assay of *Nlrc5* (right) and *Ciita* (left) promoter activity driven by IRF1 and STAT1 transfection in wild-type and *Npm1*-deficient MC38 tumor cells. Data are relative to Renilla luciferase activity. $n = 3$. (**E** and **F**) ChIP analysis of the DNA binding of IRF1 (**E**) or STAT1 (**F**) to the *Nlrc5*, *Ciita* and *Actb* promoters in wild-type and *Npm1*-deficient MC38 tumor cells with mIFN-γ stimulation (10 ng/mL) for 24 h. Data are relative to control immunoprecipitation with immunoglobulin G (IgG) antibody. $n = 3$. (**G**) The proposed model for the previously undescribed role of NPM1-IRF1-NLRC5/CIITA-MHC axis in suppressing tumor antigen presentation and reprogramming the immunosuppressive TME. Data are representative of three (**A**-**D**) or two (**E** and **F**) independent experiments. Error bars indicate mean ± SD. *P* values in **D**-**F** were calculated using a two-tailed, unpaired Student's *t* test. $^{**}P < 0.01$; $^{***}P < 0.001$. NC, negative control; WCL, whole cell lysates; TF, transcription factor; ut, untreated; n.s., not significant

previous report showed that the in vivo administration of NSC348884 robustly suppressed tumor growth but did not influence $CD8^+$ T cell infiltration [16]. We therefore hypothesize that NPM1 oligomerization is important for its pro-proliferation function, but not related to its regulation of MHC expression in tumor cells. Moreover, as a nucleolar protein, NPM1 plays critical roles in ribosome biogenesis and nucleolar organization. Systematic delivery of NPM1-targeting drugs may cause abnormal cell death of stromal cells and immune cells. Therefore, precise tumor-targeted drug delivery is required and optimal dosing and long-term effects of NPM1 inhibitors need to be explored.

Conclusions

Taken together, our results highlight a previously uncharacterized role of nucleolar protein NPM1 in promoting tumor progression and immune evasion by suppressing IRF1-mediated *Nlrc5* and *Ciita* transcription, which finally inhibits tumor cell MHC-I and MHC-II expression to impair tumor immunogenicity. *Npm1*-deficient tumors exhibit increased $CD8^+$ T cell and $CD4^+$ T cell infiltration and decreased immunosuppressive cells, indicating the critical role of NPM1 in reprogramming immunosuppressive TME.

Our findings pinpoint promising targets for improving immunotherapy responses and provide insights into how the nucleolar protein acts as a tumor intrinsic factor to reprogram the TME and promote tumor immune evasion.

Materials and methods

Mice

C57BL/6 mice (6-week-old males) were obtained from Beijing HFK Bio. All mice were bred and maintained under specific pathogen-free conditions.

Cell lines

MC38 mouse colon carcinoma cells and HCT116 human colon cancer cells were obtained from Cell Resource Center, Peking Union Medical College (PCRC) and maintained in our lab. B16F10 mouse melanoma cells, LLC mouse lung carcinoma cells and A549 human lung cancer cells were obtained from American Type Culture Collection (ATCC) and maintained in our lab. In detail, MC38, B16F10 and HCT116 cells were cultured in RPMI-1640 medium (Corning), LLC cells were cultured in DMEM medium (Corning) and A549 cells were cultured in DMEM/F12 50/50 medium (Corning), supplemented with 10% (v/v) fetal bovine serum (FBS; Gibco), 100 units/mL of penicillin and 100 μg/mL streptomycin at 37 °C, 5% CO_2.

Npm1-deficient tumor cells were generated using the CRISPR-Cas9 system, with two guide RNAs targeting intron 1 (5'-CTACATTGAGGCAACATTGC-3') and intron 2 (5'-GTCACTCCAAGGTGCTAGAT-3') at the *Npm1* locus. The efficiency of gene knockout was verified using PCR, sequencing, and immunoblotting.

Antibodies and reagents

Antibodies used in this study are listed in Table S1. Purified antibodies for the CyTOF panel were labeled with the Maxpar Antibody Labeling Kit (Fluidigm, Cat#201300) according to the manufacturer's instructions and titrated before use.

Collagenase I (Cat#17018029) and collagenase IV (Cat#17104019) were from Gibco. DNase I (Cat#DN25-1 g) was from Sigma-Aldrich. Zombie Aqua Fixable Viability Kit (Cat#423102) and FoxP3 Fix/Perm Buffer Set (Cat#421403) were from BioLegend. Recombinant mouse IFN-γ protein (CAT#485-MI) was obtained from R&D Systems. Recombinant mouse IL-2 protein (Cat#575404) was obtained from BioLegend. Recombinant human IFN-γ protein (CAT#300-02) was obtained from PeproTech. Actinomycin D (Cat#HY-17559) and NSC348884 (Cat#HY-13915) were obtained from MedChemExpress. Ovalbumin peptides (SIINFEKL) (Cat#T510212-0001) were from Sangon Biotech. Alexa Fluo 594 anti-rabbit secondary antibody (Cat#A-11012) was from Thermo Fisher Scientific. DAPI dye (Cat#4083) was from Cell Signaling Technology.

RNAi and plasmids

10 pmol siRNA mixture was transfected into $5e^4$ A549 or HCT116 cells which were plated in a 24-well plate using Lipofectamine RNAiMAX (Invitrogen, Cat#13778150)

according to the manufacturer's instructions. The sequence of siRNA for human *NPM1* is listed in Table S2. cDNA fragments encoding mouse STAT1 and IRF1 were amplified from mouse MC38 cells and cloned into the pcDNA4_myc_his_A vector. Five repeats of the core promoter region of mouse *Nlrc5* (gacagaactgaaactcagagt) or *Ciita* (gaaagtgaaagg) were synthesized by Sangon Biotech and cloned into a pGL4.17 luciferase reporter vector. All constructs were confirmed by sequencing. MC38 cells were transfected with these constructs using Lipofectamine 3000 (Invitrogen, Cat#L3000015) according to the manufacturer's instructions.

Mouse tumor models

MC38 (1×10^6 cells per mouse), B16F10 (5×10^5 cells per mouse) and LLC cells (1×10^6 cells per mouse) were cultured and harvested for subcutaneous injection in the right flank region of wild-type C57BL/6 male mice at six weeks of age. For the $CD8^+$ T cell depletion experiment, wild-type or *Npm1*-deficient MC38 tumor cells were subcutaneously injected into C57BL/6 mice on day 0 when 100 μg anti-CD8 antibody was intraperitoneally injected on days -4, -1 and 2. Tumor size was measured every 2–3 days and calculated using the formula volume = 1/2 ×(length)(width)^2. The endpoint was defined when the size of the tumor reached 1.5 cm in its longest dimension or 2000 mm^3 in volume.

Mass cytometry

Tumors were dissected from the surrounding tissue, mechanically cut and digested with collagenase I (1 mg/mL), collagenase IV (1 mg/mL) and DNase I (1 mg/mL) for 60 min at 37 °C. Cells were filtered using a 40-micrometer filter to remove clumps and resuspend in PBS at a suitable cell concentration. $CD45^+$ immune cells were isolated using mouse CD45 MicroBeads (Miltenyi Biotec, Cat#130-052-301). 0.5 μM 194Pt monoisotopic cisplatin (Fluidigm, Cat#201064) in PBS was used to distinguish between dead and living cells since cisplatin covalently binds damaged cell membranes. To ensure homogeneous staining, cells from each sample were barcoded as claimed by the manufacturer's protocols. Next, cells were incubated with FcR blocking reagent (BioLegend, Cat#101320), followed by surface staining with the indicated antibody cocktail. Cells were washed, fixed, permeabilized, and incubated with the indicated antibody cocktail for intracellular staining. Cells were washed, fixed with 1.6% formaldehyde solution (Sigma, Cat#F8775-4×25ML) and resuspended in 1 mL of nucleic acid Ir-Intercalator diluted in PBS (Fluidigm, Cat#201192A). Cells were washed and then diluted in water containing 10% EQ Four Element Calibration Beads (Fluidigm, Cat#201078). Samples were then run on the Helios Mass Cytometer (Fluidigm).

Flow cytometry

Single-cell suspensions of tumor tissues were prepared as described above. Cells were stained with indicated antibodies and then washed once with PBS for sample acquisition by the LSRFortessa (BD Biosciences) flow cytometer.

Mouse tumor cells were treated with mIFN-γ (10 ng/mL) for 48 h and stained with FITC-bound anti-mouse $H2\text{-}K^b/D^b$ antibodies and PE-bound anti-mouse $I\text{-}A^b$ antibodies for 30 min at 4 °C. Human tumor cells were treated with hIFN-γ (20 ng/mL) for 48 h and stained with PE-bound anti-human HLA-A/B/C antibodies and FITC-bound anti-human HLA-DR/DP/DQ antibodies. After washing with PBS, the surface expression of MHC-I and MHC-II were analyzed on the LSRFortessa (BD Biosciences) flow cytometer.

CTL killing assay

MC38 wild-type and *Npm1*-deficient cells were incubated with ovalbumin peptides (SIINFEKL) at 2 μg/mL for 2 h and then co-cultured with OVA-specific T cells at ratios of 1:2, 1:1, 2:1 and 4:1 for 24 h. The death of tumor cells was detected by flow analysis with PI staining (BD Pharmingen, Cat#51-66211E) or the LDH release method with CytoTox 96 Non-Radioactive Cytotoxicity Assay (Promega, Cat#G1780) as claimed by the manufacturer's instructions.

RNA extraction and quantitative RT-PCR

Total RNA was extracted from cells with TRIzol reagent (Invitrogen, Cat#15596018) according to the manufacturer's protocol. 1–2 μg acquired RNA was reverse transcribed using ReverTra Ace qPCR RT Master Mix (TOYOBO, Cat#FSQ-201). Then real-time quantitative PCR analysis was carried out with 2×RealStar Power SYBR qPCR Mix (Low ROX) (GenStar, Cat#A304-10) on QuantStudio 7 Flex (Thermo Fisher Scientific) and data were normalized by *Actb* expression in each sample using the ΔΔCt calculation method. Sequences of primers for Q-PCR were listed in Table S3.

Measurement of RNA stability

MC38 cells were stimulated with IFN-γ (10 ng/mL) for 24 h and then treated with actinomycin D (10 μg/mL) for 0, 3, 6, and 9 h. Cells were harvested to extract RNA. Reverse transcription and real-time quantitative PCR assay were performed to analyze the remaining mRNA relative to actinomycin D-untreated cells.

Immunoprecipitation (IP)

Cells were lysed with IP lysis buffer (Pierce, Cat#87787) supplemented with protease inhibitor cocktail (Millipore, Cat#539134). Anti-NPM1 antibodies were added to the same amount of protein extract and incubated overnight

at 4 °C with rotation. Then 20 μL of protein A/G magnetic beads (Pierce, Cat#88802) were added and incubated for 2 h at 4 °C. After three washes with NETN100 IP wash buffer (20 mM Tris-Cl pH 8.0, 1 mM EDTA, 0.5% NP-40, 100 mM NaCl) and one wash with NETN900 IP wash buffer (20 mM Tris-Cl pH 8.0, 1 mM EDTA, 0.5% NP-40, 900 mM NaCl), immunoprecipitated proteins were boiled for 5 min at 95 °C for immunoblotting.

Immunofluorescence

Cells were seeded onto glass coverslips in a 24-well plate and incubated overnight. After washed with PBS three times, cells were fixed with 4% polyformaldehyde solution, permeabilized with 0.5% Triton X-100 and blocked with 3% BSA. NPM1 was stained with primary antibodies and then fluorescent-dye-conjugated secondary antibodies. Nuclei were stained with DAPI dye. Fluorescence images were acquired on STED (Leica TCS SP8) confocal microscope.

Subcellular fractionation

Subcellular fractionation was performed according to a previous report [58]. In brief, cells were collected by trypsin digestion and washed twice with cold PBS. Then cells were resuspended in 500 μL 0.1% NP-40 in PBS and incubated for 5 min on ice. After spinning down at 4℃ 14,000 g for 5 min, the supernatant was taken as cytoplasmic fraction. The nuclei pellet was washed once with cold PBS. The nuclei were resuspended in 100 μL high-salt buffer (20 mM HEPES pH 7.5, 10 mM KCl, 350 mM NaCl, 1.5 mM $MgCl_2$, 1 mM EDTA, 0.1 mM Na_3VO_4, 0.2% NP-40, 10% Glycerol, 1 mM DTT, 1/200 proteinase inhibitor cocktail) and incubated on ice for 30 min. After spinning down at 4℃ 14,000 g for 20 min, the supernatant was taken as nucleoplasm fraction. The remaining pellet was resuspended in 100 μL MNase buffer (50 mM Tris-HCl, 5 mM $CaCl_2$, 1 mM DTT and 0.5 μL micrococcal nuclease) and incubated at 37℃ for 20 min. The reaction was stopped with 1 mM EDTA and centrifuged at 4℃ 14,000 g for 15 min. This final supernatant was chromatin fraction. Each fraction was loaded on SDS-PAGE gel in equal proportions.

Dual-luciferase reporter assays

Wild-type and *Npm1*-deficient MC38 cells were transfected with a mixture of *Nlrc5*-luc or *Ciita*-luc, IRF1 and STAT1 as transcriptional activators and *Renilla* luciferase as a control. Whole-cell lysates were harvested 24 h after transfection for luciferase activity measurements with the Dual-Luciferase Reporter Assay System (Promega, Cat#E1960) as stated by the manufacturer's instructions.

Chromatin immunoprecipitation (ChIP) assays

ChIP assays were performed using SimpleChIP Enzymatic Chromatin IP Kit (Cell Signaling Technology, Cat#9003) as stated by the manufacturer's instructions. Briefly, cells were cross-linked with 1% formaldehyde for 10 min at room temperature and the reaction stopped by adding glycine solution. Nuclei were isolated, followed by micrococcal nuclease digestion for 15 min at 37 °C, which was stopped with EDTA. Sonication (30-s pulse and 30-s pause, 3 cycles) was used for complete lysis of nuclei in ChIP buffer. For immunoprecipitation, digested chromatin was incubated with 7 μg of antibodies overnight at 4 °C with rotation. After that, magnetic beads were added to the immunoprecipitation reaction for 2 h at 4 °C with rotation. After being washed three times with low-salt wash buffer and one time with high-salt wash buffer, immunoprecipitated chromatin DNA was eluted and quantified using real-time quantitative PCR. Sequences of primers for ChIP Q-PCR were listed in Table S4.

Statistical analysis

Statistical tests and the number of replicates and independent experiments are listed in the text and figure legends. Data are described using mean ± SD except where indicated. Statistical analysis was performed using GraphPad Prism 8 software. *P* values of less than 0.05 were considered statistically significant. The statistical significance of tumor growth curves was analyzed using two-way ANOVA. Survival analyses were presented as Kaplan-Meier plots using the log-rank test. Correlation analyses were analyzed using Spearman correlation tests. All other statistical analyses were performed using a two-tailed, unpaired Student's *t* test.

Supplementary Information

The online version contains supplementary material available at https://doi.org/10.1186/s13045-024-01618-6.

Supplementary Material 1

Supplementary Material 2

Author contributions

X.C. supervised the study; X.W., Y.C., Y.Q., J.S. and W.Z. performed mouse experiments; X.W. performed flow cytometry, dual-luciferase reporter assays, ChIP and IP assays; Y.C. performed mass cytometry; X.X., H.X. and B.W. provided reagents and helpful discussions. X.W., J.W. and X.C. analyzed data and wrote the paper.

Funding

This work was supported by the National Natural Science Foundation of China (82388201) and CAMS Innovation Fund for Medical Sciences (2021-I2M-1-017).

Data availability

The data that support the findings of this study are available from the corresponding author upon request. RNA high-throughput sequencing data from this study are deposited in the NCBI GEO dataset under accession code GSE272634.

Declarations

Ethics approval

All mouse experiments were conducted based on the National Institutes of Health Guide for the Care and Use of Laboratory Animals, with the approval of the Animal Care and Use Committees of the Institute of Laboratory Animal Sciences of the Chinese Academy of Medical Sciences (ACUC-A02-2021-022).

Consent for publication

All authors agree to the publication of the article.

Competing interests

The authors declare no competing interests.

Received: 26 July 2024 / Accepted: 4 October 2024
Published online: 14 October 2024

References

1. Morad G, et al. Hallmarks of response, resistance, and toxicity to immune checkpoint blockade. Cell. 2021;184(21):5309–37.
2. Jhunjhunwala S, Hammer C, Delamarre L. Antigen presentation in cancer: insights into tumour immunogenicity and immune evasion. Nat Rev Cancer. 2021;21(5):298–312.
3. Kalbasi A, Ribas A. Tumour-intrinsic resistance to immune checkpoint blockade. Nat Rev Immunol. 2020;20(1):25–39.
4. Duan Q, et al. Turning cold into hot: firing up the tumor microenvironment. Trends Cancer. 2020;6(7):605–18.
5. Binnewies M, et al. Understanding the tumor immune microenvironment (TIME) for effective therapy. Nat Med. 2018;24(5):541–50.
6. Yu GJ, et al. Low-dose decitabine enhances the effect of PD-1 blockade in colorectal cancer with microsatellite stability by re-modulating the tumor microenvironment. Cell Mol Immunol. 2019;16(4):401–9.
7. Pelletier J, Thomas G, Volarevic S. Ribosome biogenesis in cancer: new players and therapeutic avenues. Nat Rev Cancer. 2018;18(1):51–63.
8. Corman A, et al. Targeting the nucleolus as a therapeutic strategy in human disease. Trends Biochem Sci. 2023;48(3):274–87.
9. Leung AKL, et al. Bioinformatic analysis of the nucleolus. Biochem J. 2003;376:553–69.
10. Andersen JS, et al. Nucleolar proteome dynamics. Nature. 2005;433(7021):77–83.
11. Iarovaia OV, et al. Nucleolus: a central hub for nuclear functions. Trends Cell Biol. 2019;29(8):647–59.
12. Grisendi S, et al. Nucleophosmin and cancer. Nat Rev Cancer. 2006;6(7):493–505.
13. Grisendi S, et al. Role of nucleophosmin in embryonic development and tumorigenesis. Nature. 2005;437(7055):147–53.
14. Wang X, et al. Mutual dependency between lncRNA LETN and protein NPM1 in controlling the nucleolar structure and functions sustaining cell proliferation. Cell Res. 2021;31(6):664–83.
15. Bertwistle D, Sugimoto M, Sherr CJ. Physical and functional interactions of the Arf tumor suppressor protein with nucleophosmin/B23. Mol Cell Biol. 2004;24(3):985–96.
16. Qin G, et al. NPM1 upregulates the transcription of PD-L1 and suppresses T cell activity in triple-negative breast cancer. Nat Commun. 2020;11(1):1669.
17. Chandrashekar DS, et al. UALCAN: an update to the integrated cancer data analysis platform. Neoplasia. 2022;25:18–27.
18. Zhu J, et al. Mesenchymal stem cells alleviate LPS-induced acute lung injury by inhibiting the proinflammatory function of Ly6C(+) CD8(+) T cells. Cell Death Dis. 2020;11(10):829.
19. Li T, et al. TIMER2.0 for analysis of tumor-infiltrating immune cells. Nucleic Acids Res. 2020;48(W1):W509–14.
20. Meissner TB, et al. NLRC5 cooperates with the RFX transcription factor complex to induce MHC class I gene expression. J Immunol. 2012;188(10):4951–8.
21. Steimle V, et al. Regulation of MHC class II expression by interferon-gamma mediated by the transactivator gene CIITA. Science. 1994;265(5168):106–9.
22. Qi W, et al. NSC348884, a nucleophosmin inhibitor disrupts oligomer formation and induces apoptosis in human cancer cells. Oncogene. 2008;27(30):4210–20.
23. Abe M, et al. Selective regulation of type II interferon-inducible genes by NPM1/nucleophosmin. FEBS Lett. 2018;592(2):244–55.
24. Kondo T, et al. Identification and characterization of nucleophosmin/B23/numatrin which binds the anti-oncogenic transcription factor IRF-1 and manifests oncogenic activity. Oncogene. 1997;15(11):1275–81.
25. McGranahan N, et al. Allele-specific HLA loss and immune escape in lung cancer evolution. Cell. 2017;171(6):1259–e127111.
26. Burr ML, et al. An evolutionarily conserved function of polycomb silences the MHC class I antigen presentation pathway and enables immune evasion in cancer. Cancer Cell. 2019;36(4):385–e4018.
27. Li GP, et al. LIMIT is an immunogenic lncRNA in cancer immunity and immunotherapy. Nat Cell Biol. 2021;23(5):526–37.
28. Yamamoto K, et al. Autophagy promotes immune evasion of pancreatic cancer by degrading MHC-I. Nature. 2020;581(7806):100–5.
29. Chan KL, et al. Inhibition of the CtBP complex and FBXO11 enhances MHC class II expression and anti-cancer immune responses. Cancer Cell. 2022;40(10):1190–e12069.
30. Han YM, et al. Tumor-induced generation of splenic erythroblast-like ter-cells promotes tumor progression. Cell. 2018;173(3):634–e64812.
31. Zhang B, et al. MFSD2A potentiates gastric cancer response to anti-PD-1 immunotherapy by reprogramming the tumor microenvironment to activate T cell response. Cancer Commun. 2023;43(10):1097–116.
32. Liu Y, Cao XT. Immunosuppressive cells in tumor immune escape and metastasis. J Mol Med. 2016;94(5):509–22.
33. Marzio A, et al. EMSY inhibits homologous recombination repair and the interferon response, promoting lung cancer immune evasion. Cell. 2022;185(1):169–e18319.
34. Duong E, et al. Type I interferon activates MHC class I-dressed CD11b conventional dendritic cells to promote protective anti-tumor CD8 T cell immunity. Immunity. 2022;55(2):308–e3239.
35. Shi QZ, et al. Increased glucose metabolism in TAMs fuels O-GlcNAcylation of lysosomal cathepsin B to promote cancer metastasis and chemoresistance. Cancer Cell. 2022;40(10):1207–e122210.
36. Lai YF et al. Dietary elaidic acid boosts tumoral antigen presentation and cancer immunity via ACSL5. Cell Metabol. 2024;36(4).
37. Bian YJ, et al. Cancer SLC43A2 alters T cell methionine metabolism and histone methylation. Nature. 2020;585(7824):277–82.
38. Peng DJ, et al. Epigenetic silencing of Th1-type chemokines shapes tumour immunity and immunotherapy. Nature. 2015;527(7577):249–53.
39. Ishizuka JJ, et al. Loss of ADAR1 in tumours overcomes resistance to immune checkpoint blockade. Nature. 2019;565(7737):43–8.
40. Waldman AD, Fritz JM, Lenardo MJ. A guide to cancer immunotherapy: from T cell basic science to clinical practice. Nat Rev Immunol. 2020;20(11):651–68.
41. Sharma P, et al. Immune checkpoint therapy-current perspectives and future directions. Cell. 2023;186(8):1652–69.
42. Hou AJ, Chen LC, Chen YY. Navigating CAR-T cells through the solid-tumour microenvironment. Nat Rev Drug Discovery. 2021;20(7):531–50.
43. Axelrod ML, et al. Biological consequences of MHC-II expression by tumor cells in cancer. Clin Cancer Res. 2019;25(8):2392–402.
44. Johnson DB, et al. Melanoma-specific MHC-II expression represents a tumour-autonomous phenotype and predicts response to anti-PD-1/PD-L1 therapy. Nat Commun. 2016;7:10582.
45. Alspach E, et al. MHC-II neoantigens shape tumour immunity and response to immunotherapy. Nature. 2019;574(7780):696–701.
46. Speiser DE, et al. CD4 T cells in cancer. Nat Cancer. 2023;4(3):317–29.
47. Tay RE, Richardson EK, Toh HC. Revisiting the role of CD4 T cells in cancer immunotherapy-new insights into old paradigms. Cancer Gene Ther. 2021;28(1–2):5–17.
48. Boulon S, et al. The nucleolus under stress. Mol Cell. 2010;40(2):216–27.
49. Carotenuto P et al. Therapeutic approaches target nucleolus cancer. Cells. 2019;8(9).
50. Frottin F, et al. The nucleolus functions as a phase-separated protein quality control compartment. Science. 2019;365(6451):342–7.
51. Herbert A, Wagner S, Nickerson JA. Induction of protein translation by ADAR1 within living cell nuclei is not dependent on RNA editing. Mol Cell. 2002;10(5):1235–46.
52. Sansam CL, Wells KS, Emeson RB. Modulation of RNA editing by functional nucleolar sequestration of ADAR2. Proc Natl Acad Sci U S A. 2003;100(24):14018–23.
53. López DJ, Rodríguez JA, Bañuelos S. Nucleophosmin, a multifunctional nucleolar organizer with a role in DNA repair. Biochim Biophys Acta Proteins Proteom. 2020;1868(12).
54. Lafontaine DLJ, et al. The nucleolus as a multiphase liquid condensate. Nat Rev Mol Cell Biol. 2021;22(3):165–82.

55. Yang K, et al. A redox mechanism underlying nucleolar stress sensing by nucleophosmin. Nat Commun. 2016;7:13599.
56. Loubeau G, et al. NPM1 silencing reduces tumour growth and MAPK signalling in prostate cancer cells. PLoS ONE. 2014;9(5):e96293.
57. Li F, et al. Epigenetic CRISPR screens identify Npm1 as a therapeutic vulnerability in non-small cell lung cancer. Cancer Res. 2020;80(17):3556–67.
58. Bi X, et al. RNA targets ribogenesis factor WDR43 to chromatin for transcription and pluripotency control. Mol Cell. 2019;75(1):102–e1169.

Publisher's note